SF2A 2019
P. Di Matteo, O. Creevey, A. Crida, G. Kordopatis, J. Malzac, J.-B. Marquette, M. N'Diaye, O. Venot (eds)

SOLAR WIND HEATING BY ALFVÉN WAVES: COMPRESSIBLE EFFECTS

V. Réville[1], M. Velli[1], A. Tenerani[1,2] and C. Shi[1]

Abstract. We study the heating produced by a compressible cascade in unidimensional solutions of the solar wind using the numerical setup described in Réville et al. (2018). Alfvén waves are injected from the photosphere and may be, depending on their frequency and amplitude, unstable to parametric decay, in which case they create a compressible cascade of forward and inward Elsässer variables. Dissipation at small scales then create an extended heat deposition in the corona, which accelerates the wind in addition to the wave pressure. This process can provide enough heating to fully sustain a solar wind solution.

Keywords: Solar wind, Alfvén Waves, Turbulence

1 Introduction

Alfvén wave turbulence is believed to be a fundamental part of the acceleration and heating of the solar wind. Particularly in the fast solar wind, spherically polarized Alfvénic perturbations are observed, *i.e* where the total magnetic field remains constant and density perturbations are weak (Belcher 1971; Tu & Marsch 1995). These perturbations nonetheless form a well developed spectrum with frequencies ranging to $10^{-6} - 10^{-1}$Hz (Bruno & Carbone 2013). If created throughout the solar wind expansion, the observed Kolmogorov-like spectrum at inertial scales must involve non-linear interactions of counter-propagating waves (Velli et al. 1989). The usual picture for incompressible turbulence goes as follows: outward going waves launched from the Sun reflects on large scale gradients of the wind velocity and Alfvén speed to create a inward component. A cascade from large scales to smaller and smaller scales occurs creating a self-similar distribution of energy and eventually leading to dissipation at kinetic scales (through for instance wave-particle interactions).

However, recent studies have shown that the fully incompressible picture may fail in the details as the heating rate obtained is not enough to fully power the solar wind. Very high resolution simulations and spectral approaches show that the incompressible perpendicular cascade heating rate is less than what phenomenological models (see e.g. Dmitruk et al. 2002) have predicted (van Ballegooijen & Asgari-Targhi 2016; Shoda et al. 2018a; Verdini et al. 2019). Moreover, Alfvén waves are known to be unstable to the parametric decay instability (PDI), when $\beta < 1$, for typical chromospheric frequencies, even considering the solar wind expansion (Tenerani & Velli 2017; Shoda et al. 2018b; Réville et al. 2018). The PDI is able to create an inward wave component through a coupling with a compressible forward sound wave and a turbulence spectrum much faster than the incompressible reflection on large scale gradients (Réville et al. 2018). Hence, this process could play an important in coronal heating as a trigger for the creation of a large scale inward component.

In this work, we look at the heating produced in simulations akin the one presented in Réville et al. (2018), where Alfvén waves are launched from the photosphere into a fully compressible MHD simulations of a flux tube. When the system is unstable to PDI, counter-propagating Alfvén and acoustic wave interact to create a turbulent cascade and heat the solution through dissipation at small scales. With enough energy flux at the photosphere, a solar wind solution can be powered only by compressible wave heating.

2 Onset of the parametric decay instability

Parametric decay is a low beta instability, where a forward Alfvén decays into a forward sound wave and an inward Alfvén wave (Galeev & Oraevskii 1963; Derby 1978; Goldstein 1978). In Réville et al. (2018), we used

[1] UCLA Earth, Planetary and Space Sciences Department, Los Angeles, CA, USA
[2] Department of Physics, University of Texas, Austin, TX, USA

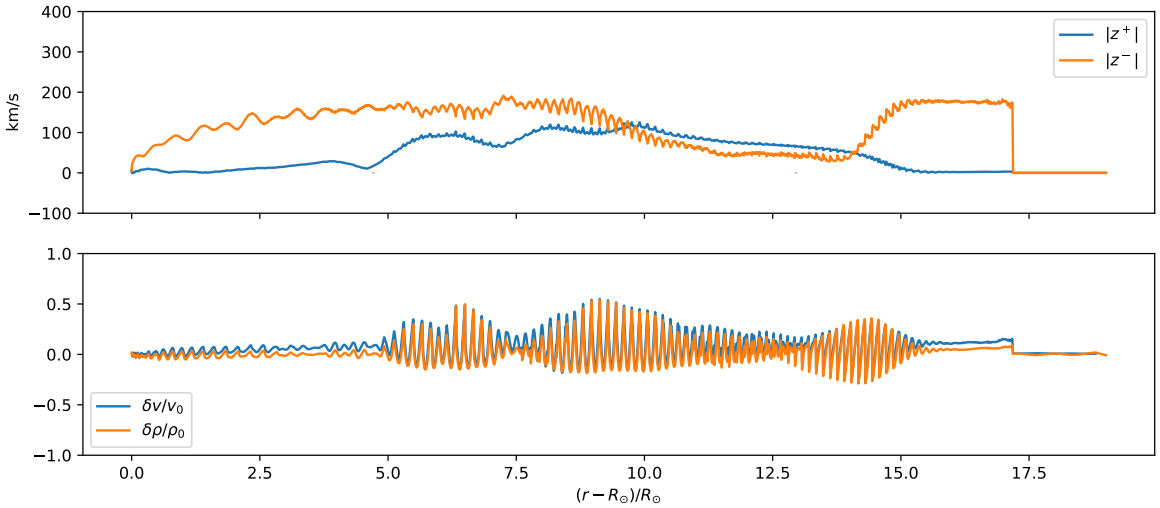

Fig. 1. Profiles of the Alfvénic perturbations ($z^\pm$) in module and of the density and velocity perturbation associated with the forward sound wave and the parametric decay. The wave front has not yet crossed the whole domain and is located at $17R_\odot$, while the instability has been triggered below $15R_\odot$.

ideal MHD simulations of a single flux tube, starting at the photosphere to show that the parametric decay instability is triggered for Alfvén waves with typical chromospheric periods (between 50 and 1000 seconds) and amplitudes of a few km/s. In Figure 1, we show the onset phase of the instability where the forward Alfvén wave (here z^-) is propagating and suddenly decays, creating a inward wave (z^+) and a forward sound wave here displayed with correlated density and velocity perturbations. We recall the definition of the Elsässer variables used here:

$$\mathbf{z}^\pm = \delta\mathbf{v}_\perp \pm \delta\mathbf{b}_\perp/\sqrt{4\pi\rho}. \tag{2.1}$$

The perturbations $\delta\rho = \rho - \rho_0$ and $\delta v = v - v_\rho$ are built with respect to the initial equilibrium profile without transverse wave (see Réville et al. 2018, for more details). We force the forward Alfvén wave from the lower boundary as:

$$\mathbf{z}^- = 2|\delta v|(\cos(\omega_0 t)\mathbf{e}_\theta + \sin(\omega_0 t)\mathbf{e}_\varphi), \tag{2.2}$$

where $\omega_0 = 2\pi f_0$ is the input pulsation.

Among the main results of Réville et al. (2018) is the demonstration that PDI is a fast process to create a well developed turbulent spectrum of both z^+ and z^- from monochromatic and non-monochromatic inputs. In Figure 2, we show the magnetic perturbations spectra computed at $10R_\odot$ for a stable and an unstable case. In these two cases a monochromatic wave is launched from the photosphere with an amplitude of $\delta v = z^-_\odot/2 = 2$ km/s. In the left panel the wave has a frequency of 10^{-3} Hz, in the right panel the input frequency is 5×10^{-3} Hz. Hence for this amplitude, the threshold for the onset of the parametric decay instability is located between these two input frequencies. For the stable case (left panel), the forward stays mostly monochromatic, while a small inward component is created through reflection on the large scale gradients. Velli et al. (1991) have indeed shown that reflection is only efficient for waves with periods larger than a few hours. In the unstable case, a significant inward wave is developed through the instability (which acts as a trigger), and a well developed spectrum is created for both component, with a clear inverse cascade exciting lower frequencies.

When the wave is unstable, the power spectra show decays roughly proportional to f^{-2}. This is related to the compressible nature of the processes occurring. Shocks are created and provide a way to dissipate energy and heat the solar wind.

3 Compressible cascade and heating of the solar wind

The pioneering work of Suzuki & Inutsuka (2005, 2006) has shown that in a similar configuration, a unidimensional solar wind solution could be self-sustained injecting Alfvén waves at the photosphere. Inside such a compressible flux tube configurations, the cascade is by definition only parallel to the magnetic field and as such omits everything happening into the perpendicular plane. Yet the numerical dissipation, associated with

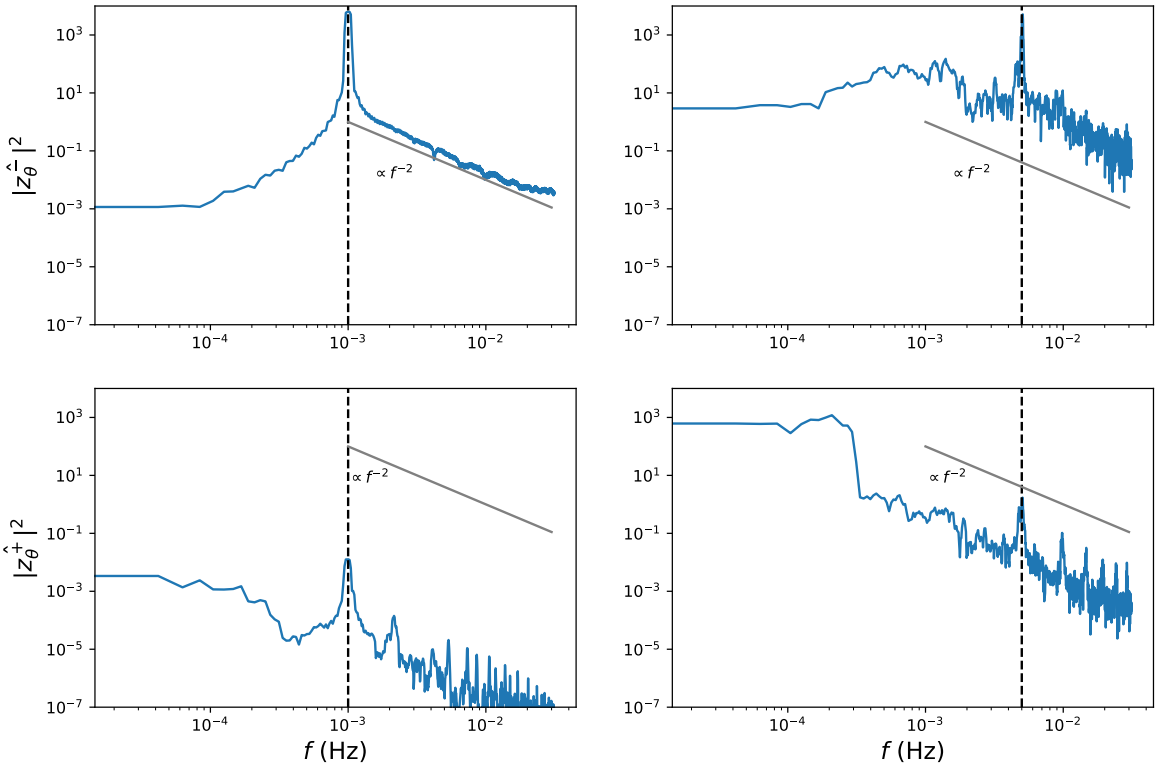

Fig. 2. Power spectra of the forward (z^+) and inward (z^-) Elsässer variable at $10R_\odot$ after three Alfvén crossing time. In the left panel the wave is launched at a frequency of 10^{-3} Hz and is therefore stable. In the right panel, the input frequency is 5×10^{-3} Hz and the instability grows, creating a inward wave of the order of the forward wave. Both component show sign of a forward and inverse cascade with slopes close to f^{-2}.

compressible effects at small scales (shocks or rotational discontinuities) in 1D, was proven to be roughly equivalent to later multi-D turbulent studies (Matsumoto & Suzuki 2012). In a recent study, Shoda et al. (2018b) compared the heating provided by shocks and compressible effects and the heating provided by a phenomenological turbulent dissipation. The study finds that depending on the correlation length scale of the turbulence the contribution of both effects vary. Compressible effects are however always very important for generating a large scale inward component and the (inverse) cascade.

In Figure 3, we compare several simulations of a solar wind flux tube with different wave inputs. In order to compare our results consistently, we fix the energy input at the photosphere. The energy flux is the combination of an ad-hoc flux that decays exponentially (over a scaleheight of $1R_\odot$, see Réville et al. 2018) and of the Alfvén wave flux. We set the total photospheric flux

$$F_{\rm tot} = F_{h,\odot} + F_{A,\odot} = F_{h,\odot} + \rho_\odot v_{A,\odot} \delta v^2 = 1.5 \times 10^5 {\rm erg.s^{-1}cm^{-2}} \tag{3.1}$$

The four cases are then split as follows: the first case (plain black curve) is the simulation without waves, the heating being only provided through the ad-hoc function. Then, two mixed cases are presented, with the energy flux split half and half between the ad-hoc function and the Alfvén wave flux (blue and orange curves). This requires $\delta v = 3.75$ km/s with the base Alfvén speed $v_{A\odot} = 3.27$ km/s and $\rho_\odot = 1.67 \times 10^{-12}$ g/cm^3. We use two different input frequencies, on both side of the parametric decay instability threshold for this amplitude. Finally the last case (red curve) is only powered through waves with $\delta v = 5.25$ km/s, and a frequency of 10^{-3} Hz, allowing a rapid onset of the PDI. In dashed black, we also show the result of the simulation without wave and with half the ad-hoc heating $F_h, \odot = 7.5 \times 10^4 {\rm erg.s^{-1}cm^{-2}}$

To compute the heating rate Q_h, we have assumed a quasi steady-state on the energy equation and wrote

$$\langle Q_h \rangle = \langle v_r \frac{\partial \rho e}{\partial r} + (\rho e + p) \nabla \cdot v_r - Q_r - Q_c \rangle, \tag{3.2}$$

where $\rho e = p/(\gamma - 1)$ and Q_r and Q_c are the radiative and the thermal conduction losses respectively.

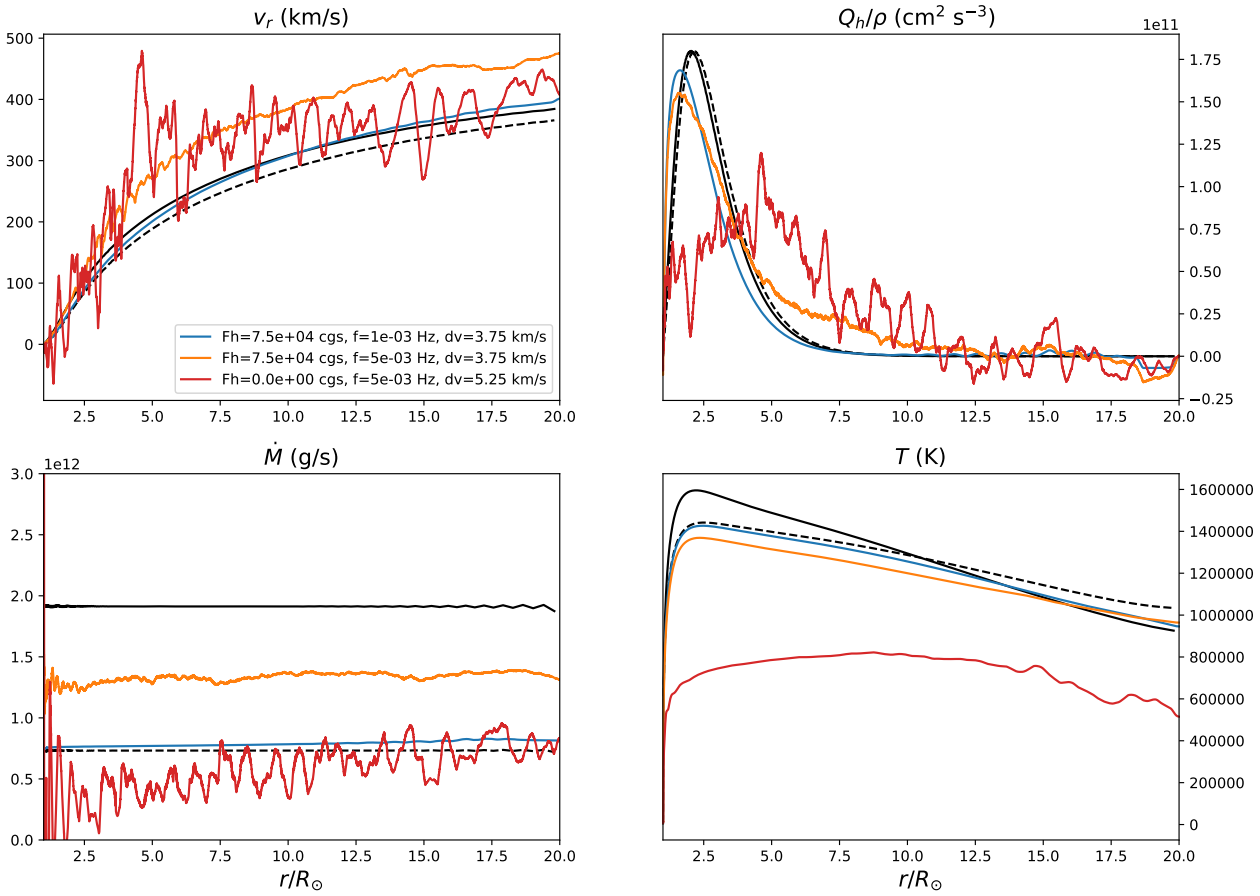

Fig. 3. Averaged speeds, heating per unit mass, mass loss and temperature for different cases in quasi steady states. The plain black curve correspond to the reference case without wave injection and $F_h = 1.5 \times 10^5$erg.s^{-1}cm^{-2}. The blue curve is a mixed case with a Alfvén wave input at stable frequencies. It notably shows the influence of wave pressure on the wind acceleration. Finally, the orange and red curve are cases where PDI develops and creates a cascade leading to heat deposition. In the red case, the heating of the corona is only maintained by the wave energy dissipation.

In Figure 3, we first notice that all our simulations are able to produce a supersonic wind. All speeds are comparable, between 300 km/s and 500 km/s at $20R_\odot$. The mass losses however are quite different. For the black curve, the heating is provided with the ad-hoc function only, and with the largest amplitude, which yields the highest mass loss. The blue curve, for which the wave is stable, yields about half the mass loss. This seems to mean that without wave heating, or for a given heat deposition profile, the mass loss is a roughly linear function of the input heat flux. Moreover, for the same amplitude of the wave but a higher frequency, the PDI is triggered and additional heating is deposited between 2 and 5 solar radii in comparison with the stable case (see the blue and orange curve in Figure 3). Because part of the energy is deposited below the sonic point, it helps lift material and indeed yields a higher mass loss. This additional heat also provide an additional acceleration of the wind. Note that the temperature of the unstable case is slightly lower as the energy is advected by the faster wind.

In the last, red, case, the heat is only provided by the compressible cascade triggered by PDI. The heating peak is more extended in the corona than in the other cases, and leads to a lower mass loss. The mass loss is approximately half the one of the no wave case, and hence is equivalent to the two other mixed cases. The temperature is however much lower, around 7.5×10^5 K at the maximum and is as such not a good proxy to determine the energy output of the wind.

4 Conclusion

In this proceeding, we have computed the heating generated by the non-linear interaction of counter-propagating Alfvén waves in a compressible simulation of a solar wind flux tube. As shown in Réville et al. (2018), the parametric decay is a very efficient way to produce inward Alfvén waves and to trigger a cascade that eventually provides heating in the solar wind solution. Although a full MHD turbulence cannot be developed in such unidimensional simulations, we can power a solar wind solution with waves only, provided that they are unstable to the parametric decay instability. Wave heating is in general more extended than the ad-hoc function, at least assuming a heating scale height of $1R_\odot$, and as such produce a faster, more tenuous wind for a given photospheric energy flux. Future works will investigate how this heating profile compares with other models of MHD turbulence including a full perpendicular cascade.

References

Belcher, J. W. 1971, ApJ, 168, 509
Bruno, R. & Carbone, V. 2013, Living Reviews in Solar Physics, 10, 2
Derby, Jr., N. F. 1978, ApJ, 224, 1013
Dmitruk, P., Matthaeus, W. H., Milano, L. J., et al. 2002, ApJ, 575, 571
Galeev, A. A. & Oraevskii, V. N. 1963, Soviet Physics Doklady, 7, 988
Goldstein, M. L. 1978, ApJ, 219, 700
Matsumoto, T. & Suzuki, T. K. 2012, ApJ, 749, 8
Réville, V., Tenerani, A., & Velli, M. 2018, ApJ, 866, 38
Shoda, M., Yokoyama, T., & Suzuki, T. K. 2018a, ApJ, 853, 190
Shoda, M., Yokoyama, T., & Suzuki, T. K. 2018b, ArXiv e-prints
Suzuki, T. K. & Inutsuka, S.-i. 2005, ApJ, 632, L49
Suzuki, T. K. & Inutsuka, S.-I. 2006, Journal of Geophysical Research (Space Physics), 111, 6101
Tenerani, A. & Velli, M. 2017, ApJ, 843, 26
Tu, C.-Y. & Marsch, E. 1995, Space Sci. Rev., 73, 1
van Ballegooijen, A. A. & Asgari-Targhi, M. 2016, ApJ, 821, 106
Velli, M., Grappin, R., & Mangeney, A. 1989, Physical Review Letters, 63, 1807
Velli, M., Grappin, R., & Mangeney, A. 1991, Geophysical and Astrophysical Fluid Dynamics, 62, 101
Verdini, A., Grappin, R., & Montagud-Camps, V. 2019, Sol. Phys., 294, 65